MODELLING A FLUIDIZED BED REACTOR BY INTEGRATING VARIOUS SCALES: PORE, PARTICLE, AND REACTOR

Robert J. Macías[1], Juan C. Maya[1], Farid Chejne[1],* Z. Afailal[2] and J. Arauzo[2],

[1]Universidad Nacional de Colombia, Facultad de Minas, Car. 80 No. 65-223,050036 Antioquia, Colombia
[2]Thermochemical Research Group (GPT), Aragón Institute of Engineering Research (I3A), University of Zaragoza, Mariano Esquillor s/n, 50018 Zaragoza, Spain

**Corresponding author*: *fchejne@unal.edu.co*

Abstract

This work proposes a novel population-balance based model for a bubbling fluidized bed reactor. This model considers two continuum phases: bubble and emulsion. The evolution of the bubble size distribution was modeled using a population balance, considering both axial and radial motion. This sub-model involves a new mathematical form for the aggregation frequency, which predicts the migration of bubbles from the reactor wall towards the reactor center. Additionally, the reacting particles were considered as a lagrangian phase, which exchanges mass with the emulsion phases. For each particle, the variation of the pore size distribution was also considered. The model presented here accurately predicted the experimental data for biochar gasification in a lab-scale bubbling fluidized bed reactor. Finally, the aggregation frequency is shown to serve as a scaling parameter.

Key Words: Fluidized bed reactor, Gasification, Population balance, Mathematical modelling

Introduction

Gasification has gained relevance in recent years and appears as an alternative for partially replacing conventional fuels since it has compounds similar to those of oil[1].

Gasification is the process of transforming coal or biomass carbonaceous material into a gaseous fuel by thermochemical reactions in various types of reactors[2]. One of the most common is the bubbling fluidized bed reactor, which has been extensively researched both experimentally and theoretically, which many industries have used for the production of energy and high added-value products[3]. In a fluidized bed, particles such as char or biomass, are suspended due to gas entering the reactor, forming a mixture of solid and gas phases with a behavior similar to that of a fluid. The excess gas produces bubbles that rise through the bed, constantly mixing the different phases. This improves the solid-gas contact, increasing the mass transfer and maintaining the temperature in the bed almost homogeneous[4].

Due to the heterogeneous nature of the fluidized beds and the strong interaction between hydrodynamics, chemical kinetics, and heat and mass transfer phenomena, it has been necessary to use empirical dimensionless group models[5] to predict the temperature and concentration profiles, char conversion, specific surface area, and porosity. However, these expressions do not consider the interaction between different phenomena and are only valid for limited reactor scales. In addition, the bubble size distribution, which is given by the characteristic bubble interactions inside the bed, is not considered by most of these models.

The first models describing the behavior of fluidized beds date back to the 50s and 70s, where the two-phase theory by Toomey and Johnstone[6] and the first fluidized-bed reactor model by Shen and Johnstone were described[7]. Subsequently, many models were published, which can be classified into two groups[8]: the simple models and the bubbling bed models. The former assume a monophasic system with three or

more variables, while the latter consider the formation of bubbles, their properties, and increasing bubble size. Horio and Wen[9] proposed a model considering two phases with adjustable parameters, which are fitted using experimental data from the center of the reactor, neglecting wall effects. Another assumption made by this model is how the variables change with vertical position within the bed. However, the model does not consider the particle size distribution. Comparing this model with experimental data demonstrated that predictability strongly depends on the adjustable experimental parameters; consequently, this model lacks generality.

In 1986, Grace[10] analyzed the performance of fluidized bed gasifiers with respect to some variables such as temperature, operating scale, heat transfer, and pressure drop. He classified the models according to the number of phases (one, two, or three) and proposed some simple expressions for the first order chemical kinetics.

In 2003, Ho[11] stated that fluidized bed gasification reactor models can be categorized into two classes. The first class refers to models based on a pseudo-homogeneous approach assuming ideal flows, a homogeneous dispersion of particles, and constant temperatures. The second class refers to models considering two phases (bubble and emulsion), where a governing equation for each phase describes the mass and energy exchange between the phases. These two-phase models have demonstrated a remarkable fit between predictions and experimental data, leading to them being the most accepted. A general expression for the mass transfer between the two phases was proposed by Wen and Fang[12]. The most used model is the so-called two-phase model proposed by Davison and Harrison[13]. This model incorporates essential phenomena such as mass transfer, hydrodynamics, bubble dynamics, and diffusion

between phases. However, this model assumes a homogenous bubble size distribution throughout the bed and is based on multiple semi-empirical correlations[14].

Over the last few years, several modifications have been introduced to the classical two-phases model[15,16]. These modifications include the modeling of bubble sizes and velocities, new equations predicting the mass transfer between phases, complex particle reactions, as well as sub-models for describing devolatilization phenomena and char conversion. Nevertheless, these models assume steady-state conditions, which does not fully represent the reality of fluidized bed gasifiers. Furthermore, certain emulsion phase particles experience intraparticle mass transfer phenomena and changes in porosity and reactivity [4,16,17] which these models do not account for.

The most common particle models do not take into consideration the effect of non-uniformity on the overall reaction rate. Recently, Maya et al. [18–21] presented several models based on population balances for predicting the evolution of microstructures during solid-gas reactions. However, these models have been used only at the particle scale without considering effects appearing at the reactor scale.

A large number of correlations have been reported in the literature for predicting the evolution of the average bubble size, and the mass transfer, heat transfer, and diffusion coefficients. However, these correlations have not been generalized and consequently lead to predictions far from experimental results when applied to the different reactors and operating conditions of the fluidized bed gasifiers[22]. The behavior of the bubbles depends on multiple operating parameters such as the reactor geometry, configuration of the distributor, and the gas velocity, physicochemical

properties, density, and viscosity. The bubble size distribution determines the dispersion of solid particles and gas within the bed, affecting the mass, heat, and momentum transfers. The above-mentioned bubble size distribution can be characterized by population balance models considering the phenomena of coalescence, rise, growth, and dispersion within the bed[23].

Several authors have explored the modelling of fluidized beds using population balances[22–25]. Models, such as proposed by Ramkrishna[26], contemplate the growth, coalescence, and rise of the bubbles within the bed. Ramkrishna's model considers that coalescence only occurs in the axial direction. However, it has been demonstrated that bubbles coalesce in both axial and radial directions by migrating towards the center of the reactor; that is, larger bubbles are concentrated in the reactor center whereas smaller bubbles are found closer to the reactor wall[27].

The coalescence of bubbles has been modeled using population balance equations by means of birth and death terms, which involves the use of a parameter known as the aggregation frequency. Some authors have proposed aggregation frequencies based on the coalescence probability as a function of vertical bubble separation[25,28–30]; however, this approach cannot be used for modelling radial coalescence.

Based on the above overview, the main shortcomings of the fluidized bed reactor models developed thus far can be summarized as: (i) omitting intra particle phenomena during gasification; and (ii) omitting radial coalesce. In consequence, the present work develops a bubbling fluidized bed model that incorporates the migration of bubbles to the reactor center due to coalescence. A population-balance based

coalescence model is coupled with the mass and heat transfer equations for both emulsion and bubble phases. Furthermore, this model considers changes in particle structure and intraparticle mass transfer phenomena. Finally, the model presents a novel mathematical form for the aggregation frequency, and modified birth and death terms in the population balance equation. The model is validated with experimental data.

Mathematical model

The correct modelling of bubbling fluidized beds implies mathematical models at various scales. Accordingly, a mathematical model predicting the behavior of CO_2 gasification in a bubbling fluidized bed reactor was proposed. Figure 1 presents a schematic of the model, which considers a dispersed phase formed by bubbles and a homogeneous phase consisting of gases and particles (emulsion).

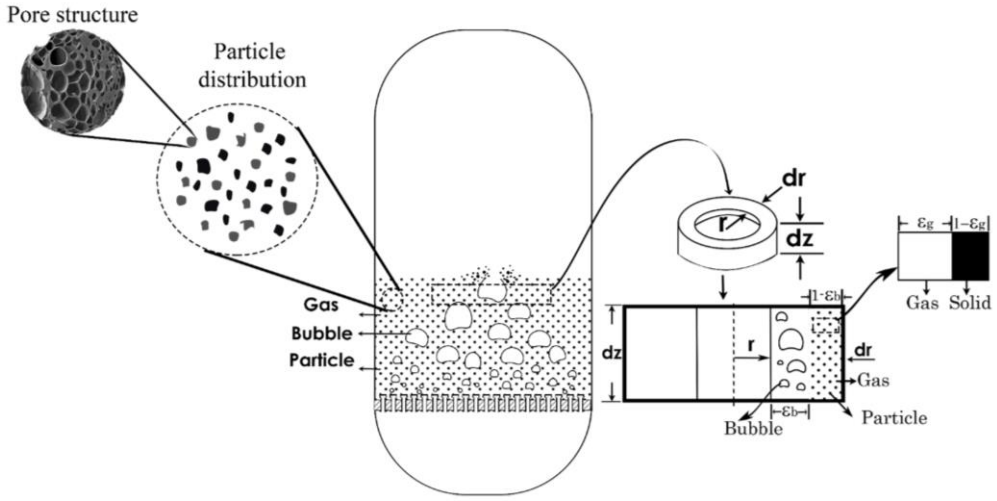

Figure 1. Schematic of fluid-dynamics processes in a bubbling fluidized bed reactor.

The particles inside the emulsion were considered as a lagrangian phase that reacts to produce a variation in the pore size distribution. The evolution of the bubble size

distribution was modeled using population balances, considering the rising of bubbles in the bed and both axial and radial motion. Mass and energy balances for each phase, as well as transfer terms between phases, were included.

Particle model

These reacting particles transfer mass to both emulsion and bubble phases along the bed. The particle model is based on that developed by Maya et al.[21], which assumes that the reactant particle is spherical and formed by cylindrical pores that grow axially when reacting with CO_2, where the reaction is given by Eq.1. The intrinsic reaction rates for the CO_2-char in terms of the change in mean pore length can be expressed by Eq.2.

$$C + CO_{2(g)} \rightarrow 2CO_{(g)} \tag{1}$$

$$\frac{dl}{dt} = \frac{k(C_{CO_2})}{\rho_m} \tag{2}$$

where l is the mean pore length, k is the kinetic constant for the CO_2-char reaction, C_{CO_2} is the CO_2 concentration, and ρ_m is the molar density of the reactant solid. The particle mass balance is calculated as:

$$\varepsilon_p \frac{\partial C_{CO_2}}{\partial t} = \frac{1}{{r_p}^2}\frac{\partial}{\partial r_p}\left(D_{eff,\mathrm{CO_2}} {r_p}^2 \frac{\partial C_{CO_2}}{\partial r_p}\right) - {\dot{r}_{\mathrm{CO_2}}}''' \tag{3}$$

$${\dot{r}_{\mathrm{CO_2}}}''' = v_C\, \rho_m \frac{dl}{dt} S \tag{4}$$

These equations account for mass transport by diffusion and chemical reaction, where ε_p is the particle porosity, r_p, C_{CO_2}, $D_{eff,\mathrm{CO_2}}$ and ${\dot{r}_{\mathrm{CO_2}}}'''$ are the particle's radial coordinate, the particle's CO_2 concentration, and the effective diffusivity and the volumetric reaction rate of the CO_2, respectively. The boundary conditions for Eq. 3 are:

$$\frac{\partial C_{CO_2}}{\partial r_p} = 0 \quad \text{at} \quad r_p=0$$

$$C_{CO_2} = C_{CO_2,e} \quad \text{at} \quad r_p=r_{p_o}$$

For the particle model, the conversion is expressed as a function of porosity as follows:

$$X(r_p, t) = 1 - \frac{(1-\varepsilon) - v_{ash}}{(1-\varepsilon_0) - v_{ash}} \tag{5}$$

where v_{ash} is the ash volume fraction. The average conversion is calculated by Eq.6.

$$\bar{X}(t) = \frac{\int_0^{r_{p_o}} 4\pi {r_p}^2 X(r_p, t) dr_p}{{}^4/_3 \pi {r_{p_o}}^3} \tag{6}$$

Pore overlapping

During the reaction process, CO_2 reacts with the carbon located at the pore ends. Consequently, the pores increase in length, which increases the specific surface area of the first stage of the reaction with CO_2. As the reaction proceeds, the pores begin to overlap, reaching a maximum specific surface area, followed by a monotonic decrease until the end of the reaction. Eq.7 gives the porosity distribution function $f_\varepsilon(r_p)$ of the extended system.

$$f_\varepsilon(r_p) = f_{\varepsilon,e}(r_p) \times \exp(-\int_0^{r_p} f_{\varepsilon,e}(r_p')\, dr_p') \tag{7}$$

Total porosity ε can be calculated as follows:

$$\varepsilon = \int_0^{\infty} f_\varepsilon\,(r_p) dr_p = 1 - \exp(-\varepsilon_e) \tag{8}$$

where ε_e is the porosity of the non-overlapped system. The non-overlapped pore system grows by a differential amount dl, where the differential change in porosity can be expressed in terms of the specific surface area of the non-overlapped system as follows:

$$d\varepsilon_e = S_e dl \tag{9}$$

The above relation is also valid for the overlapped system. Therefore, we have:

$$d\varepsilon = S\, dl \tag{10}$$

where S_e is the specific surface area of the pore ends for the non-overlapped system. Finally, the specific surface area of the pore ends for the non-overlapped system is given by:

$$S_e = \int_0^{\infty} \pi {r_p}^2 f(r_p)\, dr_p \tag{11}$$

Two-phase reactor model

The balance equations are based on the generic fluidized bed model proposed by Grace and Abba[31], which takes into account different fluidization regimes such as bubbling fluidized bed, dispersed flow at low velocities, and core-annular flow at high velocities. The mass balance for both emulsion and bubble phases includes terms of accumulation, convection, axial diffusion, interphase mass transfer, and chemical reaction. For each phase, the model considers both mass and energy transfers for predicting the evolution of both the concentration and temperature profiles over time. The equations for the emulsion and bubble phases are given by Eqs.12 and 13, respectively.

$$\frac{\partial \mathbb{C}_{i,e}}{\partial t} = -u_g \frac{\partial\, \mathbb{C}_{i,e}}{\partial z} + k_{E-B} a \left(\frac{\mathbb{C}_{i,b}(1-\epsilon_b)(\epsilon_{mf}\big)}{\epsilon_b} - \mathbb{C}_{i,e} \right) + \frac{D_{g,e}}{\epsilon_{mf}} \frac{\partial}{\partial r}\left(r \frac{\partial \mathbb{C}_{i,e}}{\partial r} \right) + \sum_j \ddot{\Gamma}_j \alpha_{i,j} + \dot{N}'''_{p-e,i} \tag{12}$$

$$\frac{\partial(\mathbb{C}_{b,i})}{\partial t} = -u_b \frac{\partial(\mathbb{C}_{bi})}{\partial z} + k_{E-B} a \left(\frac{\mathbb{C}_{e,i}\epsilon_b}{(1-\epsilon_b)\epsilon_{mf}} - \mathbb{C}_{b,i} \right) + D_{g,b} \frac{\partial}{\partial r}\left(r \frac{\partial \mathbb{C}_{i,b}}{\partial r} \right) + \sum_j \ddot{\Gamma}_j \alpha_{i,j} \quad (13)$$

where $\mathbb{C} = (C_{ei}(1-\epsilon_b)(\epsilon_{mf}))$ and $\dot{N}'''_{p-e,i}$ is the gas mass flow coming from the reactant particles, given by:

$$\dot{N}'''_{p-e,i} = 4\pi \int_0^\infty -r_{p_0}^2 f_{p(r_{p_o})} D_{eff,i} \left. \frac{dC_{co_2}}{dr_p} \right|_{r_{p_o}} dr_{p_o} \quad (14)$$

The energy balance equation for the emulsion phase and bubble phase are given by Eqs.15 and 16, respectively.

$$\frac{\partial T_e}{\partial t} = -u_g \frac{\partial T_e}{\partial z} + \frac{h_{be}}{\rho_e C p_e} a(T_b - T_e) + D_{Tg,e} \frac{\partial}{\partial r}\left(r \frac{\partial T_e}{\partial r} \right) + \sum_j \ddot{\Gamma}_j \Delta H_j + \sum_j \dot{N}'''_{p-e,i} * h_i \quad (15)$$

$$\frac{\partial T_{i,b}}{\partial t} = -u_b \frac{\partial T_b}{\partial z} + \frac{h_{be}}{\rho_b C p_b} a(T_e - T_b) + D_{Tg,b} \frac{\partial}{\partial r}\left(r \frac{\partial T_b}{\partial r} \right) + \sum_j \ddot{\Gamma}_j \Delta H_j \quad (16)$$

Population balance for the bubble size distribution

The model proposed in this work developed a population balance for the bubbles within the bed. This model explains the dynamic evolution of the bubble size distribution as a function of operating conditions. In the case of a fluidized bed reactor, the bubble size distribution may change due to coalescence between adjacent bubbles, the rising of bubbles, and the growth produced by chemical reactions. Solving the population balance equation is a difficult task; hence, this work applies the method of moments to the bubble size distribution for evaluating its effect on the surface area of

bubbles per unit volume and the volume fraction of bubbles within the reactor. The moment of the bubble size distribution function is given by:

$$M_n = \int_0^\infty f_b {r_b}^n \, dr_b \tag{17}$$

If one cylinder-shaped reactor element of cross-sectional area *Ac* and height ∆z is considered, the following balance can be made:

$$(M_n V)_{acum} = (M_n V)_{in} - (M_n V)_{out} + (M_n V)_{gen} \tag{18}$$

where $(M_n V)_{in}$ is the quantity $(M_n V)$ entering the system of volume $V = Ac \times \Delta z$, per unit time. Similarly, $(M_n V)_{out}$, $(M_n V)_{gen}$, and $(M_n V)_{acum}$ are the leaving, generation, and accumulation, respectively, of quantity $(M_n V)$ in the system of volume V per unit time. The convective flux of quantity $(M_n V)$ is given by:

$$(M_n \dot{V})'' = M_n u_b \tag{19}$$

Thus, by substituting Eq. 19 in 18, we obtain:

$$\frac{\Delta(M_n V)}{\Delta t} = (M_n u_b)_z \times Ac - (M_n u_b)_{z+\Delta z} \times Ac + (M_n V)_{gen} \tag{20}$$

Dividing both sides by V, Eq. 20 yields

$$\frac{\Delta(M_n)}{\Delta t} = \frac{(M_n u_b)_z - (M_n u_b)_{z+\Delta z}}{\Delta z} + (M_n)_{gen} \tag{21}$$

Taking the limit when both Δz and Δt tend to zero, we get:

$$\frac{\partial(M_n)}{\partial t} = \frac{-\partial(M_n u_b)}{\partial z} + (M_n)_{gen} \tag{22}$$

$(M_n)_{gen}$ appears due to coalescence and bubble growth. This term is defined elsewhere[32]:

$$(M_n)_{gen} = n\int_0^{\infty} {r_b}^{n-1}\frac{dr_b}{dt}f_b dr_b + \int_0^{\infty} {r_b}^{n}(B-D)\,dr_b \tag{23}$$

Where B and D are the birth and death terms respectively. B and D are given by:

$$B = a_{gf}\left[\frac{1}{2}\int_0^{\infty} f_b\,(r_b - r_b')f_b\,(r_b')dr_b' + f_{b\,i-1}\,(r_b)\int_0^{\infty} f_{b\,i-1}\,\left(r_b{}'\right)dr_b{}'\right] \tag{24}$$

$$D = a_{gf}\left[f_b\,(r_b)\int_0^{\infty} f_b\,(r_b')dr_b' + f_{b\,i}\int_0^{\infty} f_{b\,i}\,(r_b')dr_b'\right] \tag{25}$$

Finally, by combining Eqs. 22 and 23, we obtain:

$$\frac{\partial(M_n)}{\partial t} = \frac{-\partial(M_n u_b)}{\partial z} + n\int_0^{\infty} {r_b}^{n-1}\frac{dr_b}{dt}f_b dr_b + \int_0^{\infty} {r_b}^{n}(B-D)\,dr_b \tag{26}$$

where $M_{n,i}$ is the moment *n*, M_0 is the density (number of bubbles per unit volume), M_1 is the sum of all radius of bubbles (m of bubbles per unit volume), M_2 is proportional to the surface area of bubbles (m^2 of bubbles per unit volume), and M_3 is proportional to the porosity inside the bed (m^3 of bubble per unit volume). In addition, $\frac{dr_b}{dt}$ is the rate of change of the bubble radius due to the mass transfer between the emulsion and the bubble phase and is given by:

$$\frac{P}{RT_b}\frac{dr_b}{dt} = k_{E-B}a\left(\frac{\mathbb{C}_{e,i}\epsilon_b}{(1-\epsilon_b)\epsilon_{mf}} - \mathbb{C}_{b,i}\right) \tag{27}$$

where the specific surface area a and the volume fraction of the bubbles are expressed as follows:

$$a = 4\pi M_2 \tag{28}$$

$$\epsilon_b = \frac{4}{3}\,\pi M_3 \tag{29}$$

Furthermore, an equation for both the growth and coalescence of bubbles based on a novel form for the aggregation frequency was proposed. This model assumes that the

coalescence probability of a given bubble depends on the number of bubbles that surround it, and that bubbles migrate toward the center of the rector as coalescence takes place[33], as shown in Figure 2.

Aggregation frequency

The mathematical form for the aggregation frequency proposed in this work is based on the following assumptions.

(i) Two types of bubble coalescence: intra-element and inter-element coalescence. The former involves bubbles belonging to the same differential element, and the latter considers bubbles belonging to adjacent differential elements.

(ii) The intra-element aggregation frequency is assumed to be proportional to the bubble density in the given differential element, whereas the inter-element aggregation frequency is considered proportional to the sum of the densities of the adjacent differential elements. The latter indicates that bubbles located closer to the reactor center have a larger aggregation frequency than those located closer to the reactor wall.

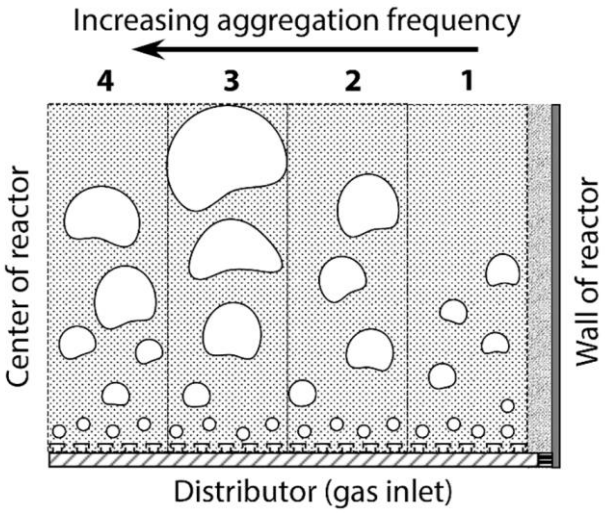

Figure 2. Representation of aggregation frequency

The inter-element bubble coalescence phenomenon is represented by new terms of birth and death, the fifth and sixth RHS terms of Eq.30. The birth term is due to the death of bubbles in the adjacent element closer to the wall. The death term is due to the coalescence of bubbles located in a given element with bubbles of the adjacent element closer to the reactor center. Therefore, it can be inferred that inter-element coalescence always drives bubbles towards the reactor center. After some mathematical manipulation, Eq. 26 takes the form of Eq.30.

$$\begin{aligned}\frac{\partial M_{n,i}}{\partial t} = -\vec{u}_b \frac{\partial M_{n,i}}{\partial z} + n\frac{dr_b}{dt} M_{n-1,i} + \frac{a_{g0} M_0}{2} \sum_{i=0}^{n} \binom{n}{i} M_{n-i} M_i \\ - a_{g0} M_0 (M_0 M_n) + \left[a_{g0}\left(M_{0,i-2} + M_{0,i}\right) M_{0,i-1} M_{n,i-1}\right] \\ - \left[a_{g0}\left(M_{0,i-1} + M_{0,i+1}\right) M_{0,i} M_{n,i}\right]\end{aligned} \tag{30}$$

The aggregation frequency a_{gf} have different mathematical forms depending on the class of coalescence. Thus, we will define the variables a_{gf_1} and a_{gf_2}, that are respectively the intra-element and inter-element aggregation frequencies, and can be calculated from:

$$a_{gf_1,i} = a_{g0} * M_{0,i} \tag{31}$$

$$a_{gf_2,i} = a_{g0} * \left(M_{0,i-1} + M_{0,i+1}\right) \tag{32}$$

where a_{g0} is a constant that must be fitted experimentally . Thus, Eq. 30 implies that the aggregation frequency near the reactor walls is smaller than that close the reactor center. Interestingly, this fact allows an approximation to the scaling of bubbling fluidized bed reactors. Firstly, let's consider the following continuity equation for the bubble size distribution function.

$$\frac{\partial f}{\partial t} + \frac{\partial (u_b f_b)}{\partial z} = B - D \tag{33}$$

by assuming a steady-state and replacing B and D from Eqs. 24 and 25, we obtain

$$\frac{\partial (u_b f_b)}{\partial z} = \overline{a_{gf}} \left[\left(\frac{1}{2} \int_0^{\infty} f_b\,(r_b - r_b')\, f_b\,(r_b')\, dr_b' + f_{b\,i-1}\,(r_b) \int_0^{\infty} f_{b\,i-1}\,(r_b')\, dr_b' \right) - \left(f_b\,(r_b) \int_0^{\infty} f_b\,(r_b')\, dr_b' + f_{b\,i} \int_0^{\infty} f_{b\,i}\,(r_b')\, dr_b' \right) \right] \tag{34}$$

It must be said, that in this case averaged aggregation frequency $\overline{a_{gf}}$ is for the sake of deriving dimensionless parameters useful for the scaling up process. The average aggregation frequency is defined by:

$$\overline{a_{gf}} = \frac{\int_0^{r_0} a_{gf}\big|_{z=0} 2\pi r dr}{\pi {r_0}^2} \tag{35}$$

From Eq.35 it is inferred that as the reactor radius increases, the average aggregation frequency also increases. Conversely, as the reactor radius decreases, the average aggregation decreases too. This lattes suggest that the average aggregation frequency can be used in the scaling up process. Now, the following set of dimensionless variables are defined.

$${r_b}'^{*} = \frac{r_b'}{\overline{r_{b_0}}}\ ; \qquad {u_b}^{*} = \frac{u_b}{u_{b\,0}}\ ; \qquad z^{*} = \frac{z}{H}\ ; \qquad {r_b}^{*} = \frac{r_b}{\overline{r_{b_0}}}\ ; \qquad {f_b}^{*}(r_b) = \frac{f_b\,(r_b)}{f_{b\,0}} \tag{36}$$

where $\overline{r_{b_0}}$, $u_{b\,0}$ and $f_{b\,0}$ are respectively the average bubble radius, the bubble velocity, and the bubble radius distribution function at $z = 0$. By substituting variables of Eq. 36 in Eq.34, we have:

$$\frac{\partial(u^* f_b{}^*)}{\partial z^*} = \frac{\overline{a_{gf}} H f_{b_0} \overline{r_{b_0}}}{u_0} \left[\left(\frac{1}{2} \int_0^\infty f_b{}^* (r_b - r_b{}') f_b{}^* (r_b{}') dr_b{}'^* \right. \right. \tag{37}$$

$$\left. + f_{b\,i-1}{}^* (r_b) \int_0^\infty f_{b\,i-1}{}^* (r_b{}') dr_b{}'^* \right)$$

$$\left. - \left(f_b{}^* (r_b) \int_0^\infty f_b{}^* (r_b{}') dr_b{}'^* + f_{b\,i}{}^* \int_0^\infty f_{b\,i}{}^* (r_b{}') dr_b{}'^* \right) \right]$$

In Eq.37, is observed, a dimensionless number appears, is defined as follows:

$$\psi = \frac{\overline{a_{gf}} H f_{b_0} \overline{r_{b_0}}}{u_{g_0}} \tag{38}$$

This dimensionless number ψ relates the characteristic time for bubble rising $\tau_u = \frac{H}{u_{g_0}}$ with the characteristic time for bubble coalescence $\tau_a = \frac{1}{\overline{a_{gf}} f_{b_0} \overline{r_{b_0}}}$ as follows:

$$\psi = \frac{\tau_u}{\tau_a} \tag{39}$$

Thus, the dimensionless number ψ allows to relate the forces involved with the bubble rising with those related to the bubble migration from the reactor walls to the center. In this sense, it is expected that maintaining this dimensionless number the bubbling regime will be conserved. The above dissertation does no pretend to establish a new validated scaling up process but to demonstrate that from the population balance modelling it is possible to explore new alternatives for scaling up bubbling fluidized bed reactors.

Solution method and scales connection strategy

The present mathematical model was solved using the software ode15s of Matlab R2019b, which is a solver of stiff ordinary differential equations that allows for the

coupling of algebraic equations. Partial spatial derivatives are discretized by centered finite differences for diffusive terms and by the upwind scheme for convective terms.

The energy and mass balance equations for all the phases and population balances for the bubbles were coupled. The emulsion phase was coupled to the bubble phase by the second RHS term of Eqs.12, 13, 15 and 16. The emulsion phase was coupled to the particles by the fifth RHS term of Eqs. 12 and 15. Finally, the population balance was connected by Eqs. 28 and 29.

Results and discussions

The model was initially validated with experimental data obtained from the scientific literature. This validation was further complemented with experimental tests in both a fluidized bed reactor and a thermobalance. Finally, some model predictions of the steady state bed porosity, mean bubble size, temperature, and pressure fluctuations within the bed were analyzed.

The present work's model predictions were fitted to experimental data reported by Rüdisüli et al.[34,35], which were obtained in a fluidized bed reactor without chemical reaction. They measured the frequency and distribution of the bubbles in a bubbling fluidized bed using optical sensors, finding that the bubbles migrated from the walls towards the center of the bed and that larger bubbles tended to be located in the upper part of the bed. The following figures compare the experimental data obtained by Rüdisüli et al[35], the results of the model developed here.

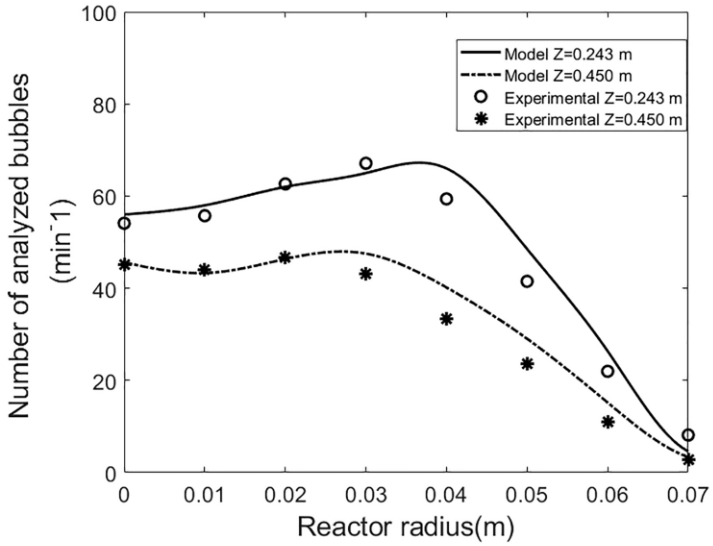

Figure 3. Bubble frequency predictions

Figure 3 shows that bubbles migrate to the reactor center, as predicted by the additional birth and death terms in the present model related to the migration of bubbles between bins. Figure 3 also shows that the number of bubbles is larger at Z=0.243 m that at Z=0.450 m. This is due to the coalescence phenomenon, which leads to a decrease in the number of bubbles with increasing height within the reactor.

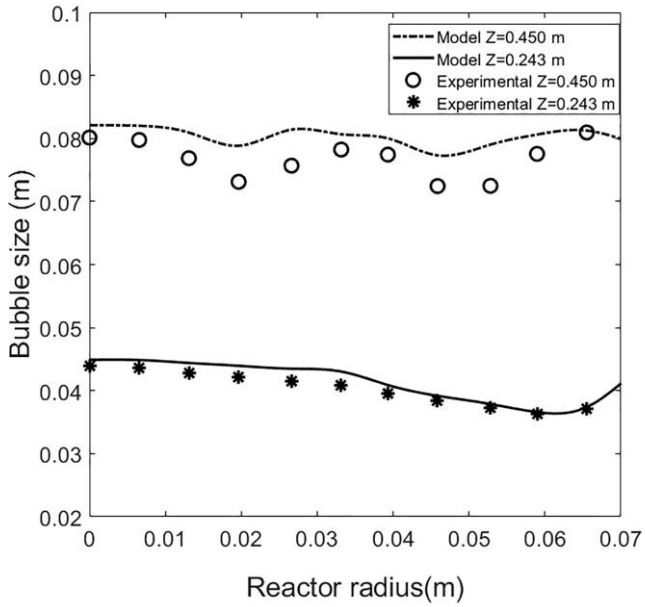

Figure 4. Bubble size predictions

Figure 4 presents the bubble size profile at two different heights within the bed, showing the model to predict the experimental data remarkably well. This figure indicates that the bubble size increases with increasing height within the bed. This is due to the coalescence phenomenon, which decreases the number of bubbles while increasing the average bubble radius.

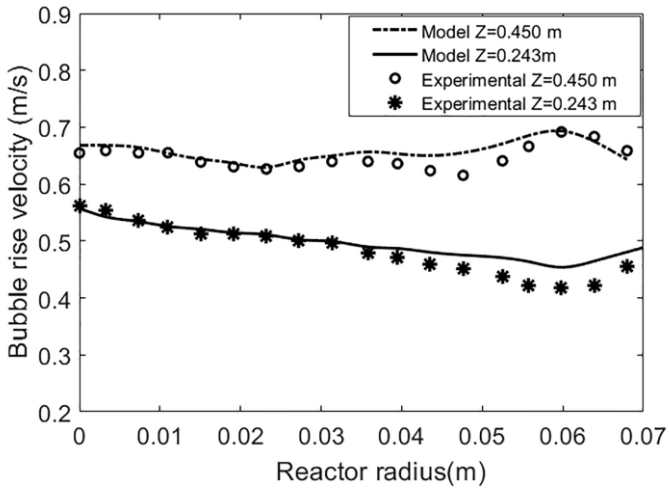

Figure 5. Bubble rise velocity predictions

Figure 5 presents the bubble rise velocity profile at two reactor heights, showing greater velocity with increasing height within the reactor. This is due to the bubble size increase, and, as observed in Figure 4, the larger bubbles are located higher within the reactor.

Subsequently, the model predictions were compared with experimental data of the CO_2-char reaction, taken in both a fluidized bed reactor and a thermobalance. Char gasification experiments were realized at the Aragón Institute for Engineering Research (I3A), Universidad de Zaragoza. In these experiments, char particles were gasified using CO_2 as a gasifying agent at an operating temperature of 900 °C. The material used in this study was obtained from Encino biomass pyrolysis, it was characterized in terms of composition, calorific value and BET specific surface area.

Table 1 resumes the results of the ultimate and the proximate analyses, the heating value and the specific surface area. Analytical standards and methods used in the material's characterization are given too in the Table 1.

The gasification experiments were conducted in a laboratory-scale fluidized bed reactor (1.27m height and 0.04m diameter) operating at atmospheric pressure shown in Figure 6. The reactor heating was assured in N_2 atmosphere, then once the temperature rose 900 °C, before solid alimentation, the change from N_2 atmosphere to CO_2 was provided via gas valves situated in the reactor bottom. Solid was fed from the upper part of the reactor through double valve feeding system. Small particles of char were retained at the level of cyclone (at temperature up to 600 ºC) and gloss wool hot filter (at 450 ºC). Condensable gases produced were collected in the condenser cooled at 0 ºC through a water-recirculating chiller, then the small aerosols were retained from non-condensable gases using a cotton filter. The volume of gas produced was measured by a volumetric meter. Gas composition was analyzed continuously using a micro gas chromatograph (Agilent 3000-A). Once the experiment finished, the reactor was leaved cooling under nitrogen atmosphere.

As for raw material, for each fluidized bed gasification experiment, the specific surface area of the produced solid was determined.

Table 1. Characterization of char sample

Proximate analysis (wt. % wet basis)		**Analytical standard or equipment**
Moisture	5.55±0.03	EN 14774-3:2010
Ash	12.8±0.3	EN 14775:2010
Volatile matter	29.4±0.1	EN 15148-2010
Fixed carbon	52.3±0.2	By difference
Heating Value (MJ/kg) (dry basis)		

HHV	24.8±42.4	Calorific Bomb IKA C2000
LHV	24.1±42.4	basic
Ultimate analysis (wt. % wet basis)		
C	68.56±0.01	LECO CHN628
H	3.24±0.05	LECO CHN628
N	0.75±0.03	LECO CHN628
S	<0.05	LECO CHN628- 628-S add-on
O	14.69±0.03	By difference
Area (m2/g)		Quantachrome Autosorb iQ gas sorption
Total area	205.00	

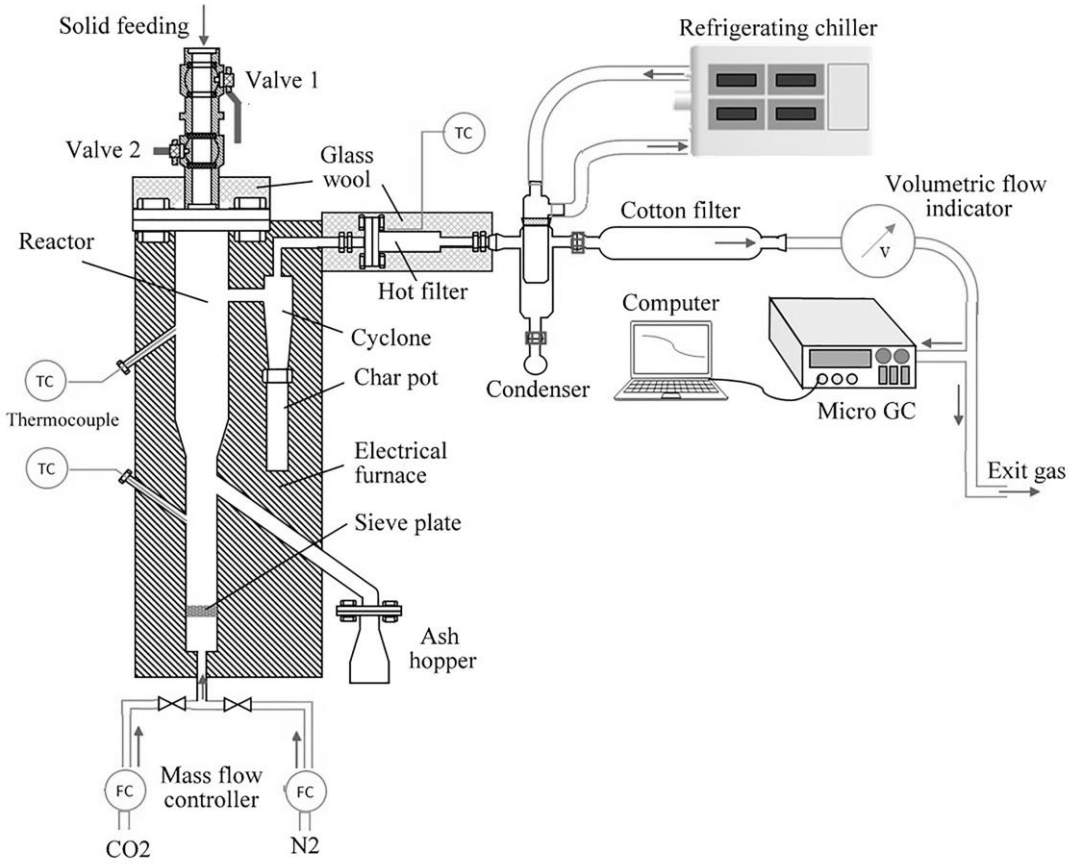

Figure 6. Diagram of fluidized bed experimental setup

The present model requires known intrinsic kinetics. Therefore, five tests (in duplicate) were carried out with a thermogravimetric balance (TGA-DTG, Proteus STA 449 F1 Jupiter- Netzsch) to determine the intrinsic kinetics of the reaction (pre-exponential

factor, activation energy and reaction order). During these tests, around 20 mg of the solid sample was heated at a constant heat rate of 10°C/min from ambient temperature to the chosen temperature, then it was maintained during 1h. The temperature (800, 850 and 900 °C) and composition of the gasifying agent CO_2/N_2 (50-50%, 70-30% and 30-70%) were varied and the experimental data were fitted to the model under chemical control conditions. The evolution of both specific surface area with conversion and with the time of the particles in the fluidized bed reactor are shown in Figure 7(a) and Figure 7(b), respectively.

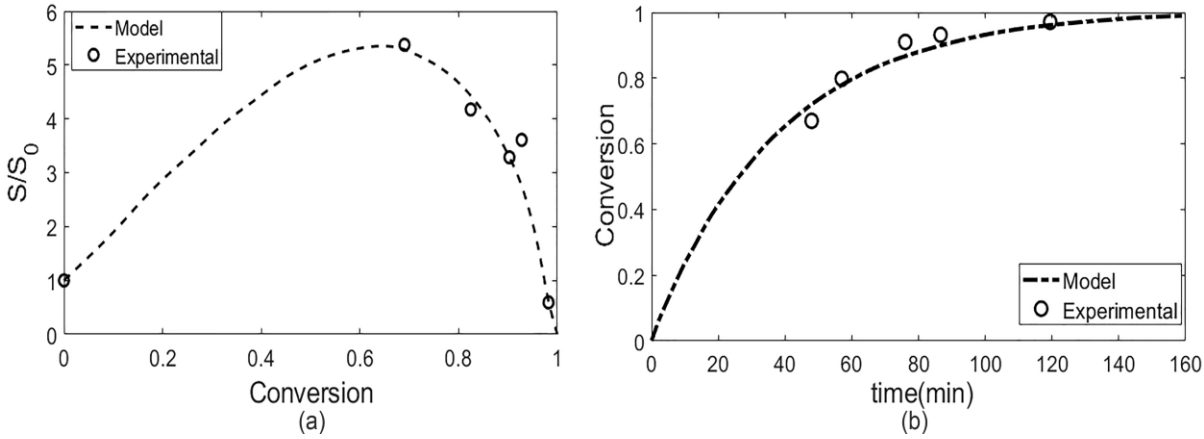

Figure 7. a) Evolution of specific surface area with conversion. b) Evolution of char conversion over time.

Figure 7(a) shows the evolution of specific surface area with conversion, indicating that it reaches a maximum before decreasing with further conversion. At the initial stages of gasification, the reaction induces pore growth, increasing the specific surface area of the reacting particle. However, as gasification progresses, the pores begin to overlap with adjacent pores. Consequently, there is a moment when pore overlapping becomes dominant, resulting in a decrease of the specific surface area. Figure 7(b) presents the evolution of conversion with time, showing that the conversion fraction with the maximum specific surface area (X=0.71) corresponds to 28% of the time

required for completing the reaction. Therefore, in order to obtain a char with high specific surface area (for instance. activated coal), long reaction times must be avoided.

Finally, some predictions of the present model are analyzed. A fluidized bed reactor was modeled in the steady-state at 850 °C with 1 mm diameter char particles. The fluidized bed reactor has a radius of 0.3 m and a bed height of 0.4 m. Results were modeled at a height of 0.3 m above the distributor, predicting the variation of both the bubble size distribution and bed porosity at different ratios of minimum fluidization velocities.

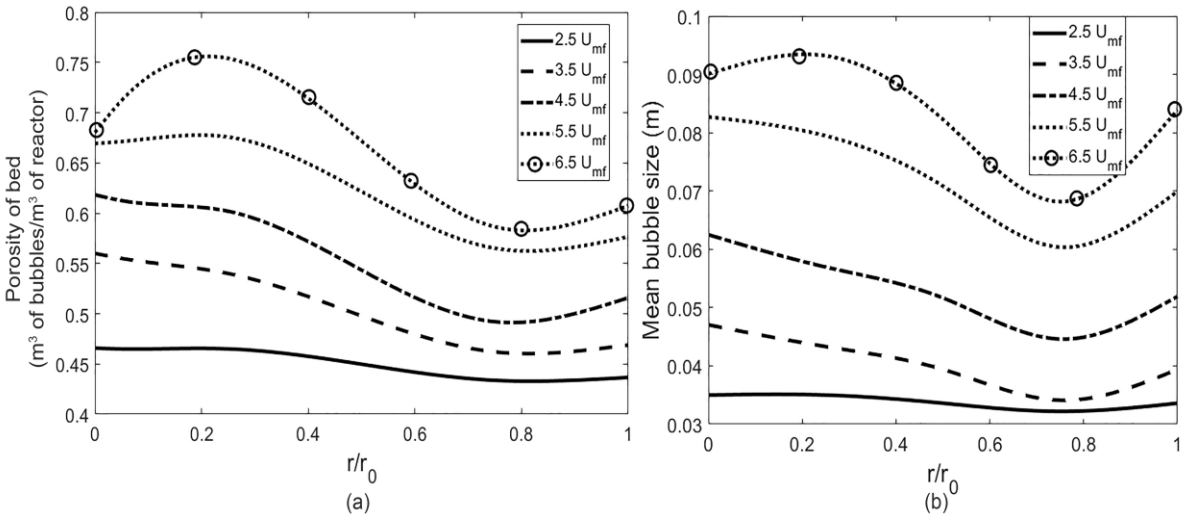

Figure 8. (a) Porosity distribution and (b) Average bubble size with radial position for various fluidization velocities

Figure 8 (a) presents the porosity profiles for various fluidization velocities. The porosity at the reactor center is larger than that at the reactor walls, due to the bubbles located close to the reactor walls migrating towards the reactor center as coalescence takes place. Furthermore, the porosity in the reactor increases with increasing flow velocity as well. This is due to the excess gas producing a greater number of bubbles.

Additionally, a higher gas velocity results in a greater reactivity and consequently increased bubble growth. Figure 8 (b) presents the mean bubble size profile. The mean bubble size increases with increasing fluidization velocity, also due to the greater number of bubbles resulting from the excess gas. Consequently increasing the aggregation frequency, as well. The figure further shows that larger bubbles are located in the center of the reactor, whereas smaller bubbles are found closer to the reactor wall. This is due to the inter-element coalescence phenomenon, by which the bubbles migrate from the wall towards the center of the reactor.

Moreover, the temperature profiles of emulsion for various flow velocities were simulated, presented in Figure 9. The profiles are almost flat, indicating that the radial heat transfer is negligible. On the other hand, the average temperature within the bed increases with increasing gas velocity. This is due to the heat transfer between the bubble and emulsion phases improving with the greater number of bubbles and therefore bubble surface area coming from the distributor as the flow velocity increases.

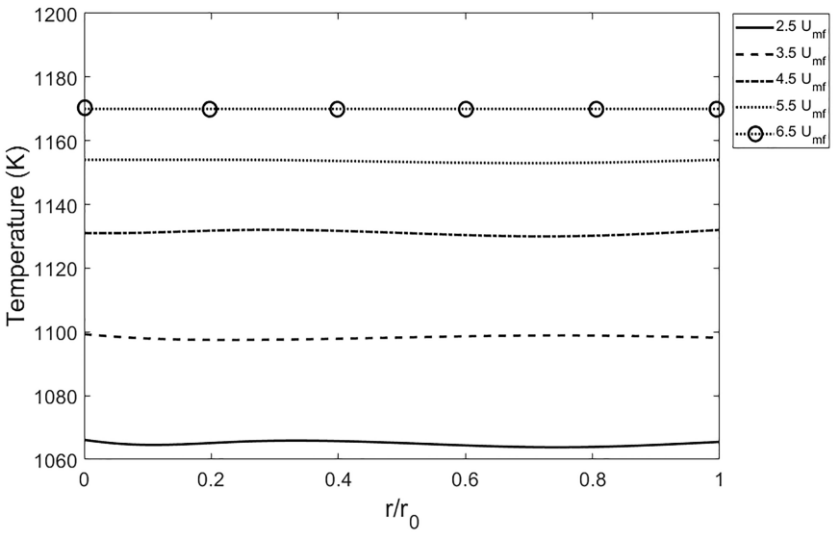

Figure 9. Emulsion temperature profiles

Finally. Figure 10 presents the pressure with time at z=0.3 m. Initially, there is an abrupt drop in pressure near time zero, due to the increase in bed porosity with the initial gas flow across the distributor. Subsequently, the pressure continues to decrease due to the chemical reaction, exhibiting a greater rate of decrease as the reaction progresses.

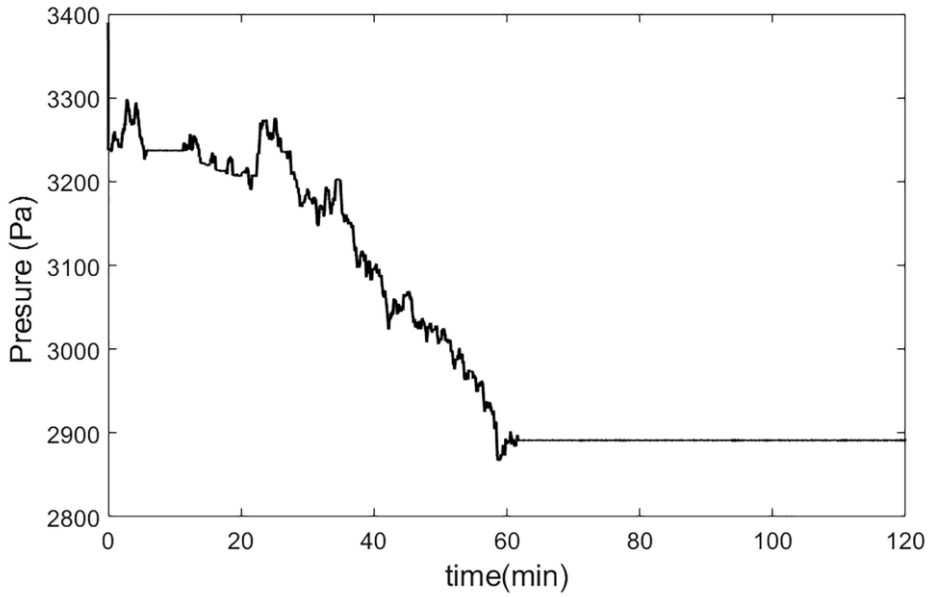

Figure 10. Evolution of pressure over time at z=0.3 m.

The above predictions are in agreement with experimental observations of bubble migration from the walls to the reactor center [25,27,28,36,37]. Notably, this phenomenon has not been modeled previously. Consequently constituting the main scientific contribution of the present work.

Concluding remarks

The present work proposes a novel population-balance based model incorporating the effect of bubble coalescence on the evolution of the bubble size distribution. The equations of the developed model were solved simultaneously, integrating reactivity,

hydrodynamics as well as energy and mass transfers simulating the dynamics of a bubbling fluidized bed at different scales: pore, particle and reactor. This model was successfully validated with experimental data.

A new mathematical form for the aggregation frequency is proposed, simulating the phenomena of intra-bin and inter-bin coalescence. This aggregation frequency depends on the bubble density within a given element in the case of intra-element coalescence and on the adjacent element bubble density in the case of inter-element coalescence. The mathematical form proposed in this work predicts the bubble migration from the reactor wall towards the center. This phenomenon has been observed experimentally, however it had not been modelled previously. Consequently, its successful prediction is a significant contribution of this work. In addition, the aggregation frequency can be used as a parameter for the scaling of fluidized bed reactors representing another significant contribution of this work.

Acknowledgments

The first author would like to thank call 785 of Colciencias “Convocatoria de Doctorados Nacionales 2017”. The Universidad Nacional de Colombia, as well as Universidad de Zaragoza for their support. Furthermore, the authors wish to thank the project "Strategy of transformation of the Colombian energy sector in the horizon 2030", funded by call 788 of Colciencias Scientific Ecosystem. Contract number FP44842-210-2018. Jesús Arauzo acknowledges the funding from the Aragón Government (ref. T22_20R), co-funded by FEDER 2014-2020 “Construyendo Europa desde Aragón”.

Notation

a_{g0} Aggregation frequency. 1/m3-s

a Surface area of bubbles per unit volume. m^2/m^3

B Birth term in the population balance equation

$\mathbb{C}_{i.e}$ Concentration of species *i* in emulsion phase. mol/m^3 reactor

$\mathbb{C}_{i.b}$ Concentration of species *i* in bubble phase. mol/m^3 reactor

C_{CO_2} Concentration of CO2 in the particle

Cp_e Average specific heat of the emulsion phase. (J/kg-K)

Cp_b Average specific heat of the bubble phase. (J/kg-K)

D Death term in the population balance equation

$D_{eff.\mathrm{CO}_2}$ Effective diffusivity of CO2

$D_{g.i}$ Gaseous dispersion coefficients, axially and radially for emulsion and bubble phase (i=e and i=b). m^2/s

$D_{Tg.e}$ Heat diffusivity of gas i in the emulsion phase. (m^2/s)

$D_{Tg.b}$ Heat diffusivity of gas i in the bubble phase. (m^2/s)

f_b Density distribution function of bubble radius. number of bubbles/m^3 reactor- m of bubble radius

h_i Specific enthalpy of the gas i. J/mol

h_{be} Heat transfer coefficient between bubble and emulsion phases. W/m^2-K

H Height of bed. m

k_{E-B} Mass transfer coefficient between emulsion and bubble phases. m/s

k_1 is the reaction kinetic constants for the CO2-char

L length. m

l Average pore length. m

M_n n-th moment (n=0.1.2.3…). m^n/m^3 of reactor

$M_{n.i}$ n-th moment of bin i. m^n/m^3 of reactor

$\dot{N}'''_{p-e.i}$ Flow of the gas i from the particle per unit volume. mol/m^3-s

r Radial coordinate within the reactor. m

r_0 Reactor radius. m

r_p Radial coordinate of particle

r_b Bubble radius. m

$\mathrm{r_{p_0}}$ Particle radius. m

S Specific surface area of particle. m^2/m^3

S_e Specific surface area of the extended pore system. m^2/m^3

S_0 Specific surface area at the beginning of reaction. m^2/m^3

T_i Temperature of phase i (i=e and i=b). K

u_b Bubble velocity. m/s

u_g Gas velocity. m/s

X Conversion

z Axial coordinate of bed height. m

$\alpha_{i.j}$ Stoichiometric coefficient of the gas i in the reaction j

$\ddot{\Gamma}_j$ j-th volumetric reaction rate. $kmol/m^3$-s

ΔH_j Heat of reaction j. J/mol

ρ_b Density of the bubble phase. kg/m^3

ρ_e Density of the emulsion phase. kg/m^3

ϵ_{mf} Volume fraction of bubbles for the minimum fluidization velocity. m^3 of bubbles/m^3 of reactor

ϵ_b Volume fraction of bubbles within reactor. m^3 of bubbles/m^3 of reactor

ε_p Porosity of particle. m^3 of pore/ m^3 of particle

v_C is the volumetric fraction of carbon in the particle

References

1. Meerman JC, Knoope M, Ramírez A, Turkenburg WC, Faaij APC. The Techno-Economic Potential of Integrated Gasification Co-Generation Facilities with CCS Going from Coal to Biomass. *Energy Procedia*. 2013;37:6053-6061. doi:10.1016/j.egypro.2013.06.534
2. Higman C, Burgt M van der. *Gasification*. Gulf Professional Pub./Elsevier Science; 2008.
3. Basu P. *Biomass Gasification and Pyrolysis*. Vol 45. (Basu P, ed.). © 2010 Elsevier Inc.; 2010. doi:10.1016/B978-0-12-374988-8.00011-8
4. Rüdisüli M, Schildhauer TJ, Biollaz SM a., van Ommen JR. Scale-up of bubbling fluidized bed reactors — A review. *Powder Technol*. 2012;217:21-38. doi:10.1016/j.powtec.2011.10.004
5. Horio M, Nonaka A, Sawa Y, Muchi I. A new similarity rule for fluidized bed scale-up. *AIChE J*. 1986;32(9):1466-1482. doi:10.1002/aic.690320908
6. Knowlton TM. Fluidized Bed Technologies for Near-Zero Emission Combustion and Gasification. *Fluid Bed Technol Near-Zero Emiss Combust Gasif*. 2013:481-523. doi:10.1533/9780857098801.2.481
7. Mahecha-Botero A, Grace JR, Elnashaie SSEH, Lim CJ. Advances in modeling of fluidized-bed catalytic reactors: A comprehensive review. *Chem Eng Commun*. 2009;196(11):1375-1405. doi:10.1080/00986440902938709
8. Grace JR. An evaluation of models for fluidized bed reactors, in: Fluidization

fundamental studies, solid-fluid reactions, and applications. *Am Inst Chem Eng*. 1971:159-157.

9. Horio M, Wen CY. An assessment of fluidized bed modeling. *Fluid Theor Appl*. 1977;73:9-21.
10. Geldart D. *Gas Fluidization Technology*. Wiley; 1986.
11. Yang W-C. Handbook of fluidization and fluid-particle systems. *China Particuology*. 2003;1(3):137.
12. Wen C-Y, Fan LT (Liang-tseng). *Models for Flow Systems and Chemical Reactors*. Dekker; 1975.
13. Davidson JF (John F, Harrison D (David). *Fluidised Particles,*. University Press; 1963.
14. Knowlton TM. Fluidized Bed Technologies for Near-Zero Emission Combustion and Gasification. In: *Fluidized Bed Technologies for Near-Zero Emission Combustion and Gasification*. Elsevier; 2013:481-523. doi:10.1533/9780857098801.2.481
15. Mahecha-Botero A, Grace JR, Elnashaie SSEH, Lim CJ. ADVANCES IN MODELING OF FLUIDIZED-BED CATALYTIC REACTORS: A COMPREHENSIVE REVIEW. *Chem Eng Commun*. 2009;196(11):1375-1405. doi:10.1080/00986440902938709
16. Gómez-Barea a., Leckner B. Modeling of biomass gasification in fluidized bed. *Prog Energy Combust Sci*. 2010;36(4):444-509. doi:10.1016/j.pecs.2009.12.002
17. Tomeczek J, Kudzia W, Gradonń B, Remarczyk L. The influence of geometrical factors and feedstock on gasification in a high temperature fluidised bed. *Can J Chem Eng*. 1987;65(5):785-790. doi:10.1002/cjce.5450650512

18. Maya JC, Chejne F, Gómez CA, Bhatia SK, Janna FC. Effect of the CaO sintering on the calcination rate of CaCO3 under atmospheres containing CO2. *AIChE J*. 2016;142(10):3638-3648. doi:10.1021/ef5012403
19. Maya JC, Chejne F, Bhatia SK. Novel model for the sintering of ceramics with bimodal pore size distributions: Application to the sintering of lime. *AIChE J*. 2017;63(3):893-902. doi:10.1002/aic.15446
20. Maya JC, Chejne F, Bhatia SK. On the modeling of the co2-catalyzed sintering of calcium oxide. *AIChE J*. 2017;63(8):3286-3296. doi:10.1002/aic.15696
21. Maya JC, Macías R, Gómez CA, Chejne F. On the evolution of pore microstructure during coal char activation with steam/CO2 mixtures. *Carbon N Y*. 2020;158:121-130. doi:10.1016/j.carbon.2019.11.088
22. Bhole MR, Joshi JB, Ramkrishna D. Population balance modeling for bubble columns operating in the homogeneous regime. *AIChE J*. 2007;53(3):579-588. doi:10.1002/aic.11099
23. Solsvik J, Jakobsen HA. Bubble Coalescence Modeling in the Population Balance Framework. *J Dispers Sci Technol*. 2014;35(11):1626-1642. doi:10.1080/01932691.2013.866902
24. Ahmadzadeh A, Arastoopour H, Teymour F, Strumendo M. Population balance equations' application in rotating fluidized bed polymerization reactor. *Chem Eng Res Des*. 2008;86(4):329-343. doi:10.1016/j.cherd.2008.02.004
25. Muralidhar R, Gustafson S, Ramkrishna D. Population balance modelling of bubbling fluidized beds. II. Axially dispersed dense phase. *Sadhana*. 1987;10(1-2):69-86. doi:10.1007/BF02816198
26. Sweet IR, Gustafson SS, Ramkrishna D. Population balance modelling of bubbling fluidized bed reactors—I. well-stirred dense phase. *Chem Eng Sci*.

1987;42(2):341-351. doi:10.1016/0009-2509(87)85064-9

27. Movahedirad S, Molaei Dehkordi A, Deen NG, van Sint Annaland M, Kuipers JAMH. Novel phenomenological discrete bubble model of freely bubbling dense gas-solid fluidized beds: Application to two-dimensional beds. *AIChE J*. 2012;58(11):3306-3317. doi:10.1002/aic.13729
28. Sweet IR, Gustafson SS, Ramkrishna D. Population balance modelling of bubbling fluidized bed reactors—I. well-stirred dense phase. *Chem Eng Sci*. 1987;42(2):341-351. doi:10.1016/0009-2509(87)85064-9
29. Shah BH, Ramkrishna D, Borwanker JD. Simulation of bubble populations in a gas fluidized bed. *Chem Eng Sci*. 1977;32(12):1419-1425. doi:10.1016/0009-2509(77)80238-8
30. Argyriou DT, List HL, Shinnar R. Bubble growth by coalescence in gas fluidized beds. *AIChE J*. 1971;17(1):122-130. doi:10.1002/aic.690170126
31. Abba IA, Grace JR, Bi HT, Thompson ML. Spanning the flow regimes: Generic fluidized-bed reactor model. *AIChE J*. 2003;49(7):1838-1848. doi:10.1002/aic.690490720
32. Maya JC, Janna FC. Novel model for non catalytic solid–gas reactions with structural changes by chemical reaction and sintering. *Chem Eng Sci*. 2016;142:258-268. doi:10.1016/j.ces.2015.11.036
33. Darton R, LaNauze R, Davidson J, Harrison D. Bubble growth due to coalescence in fluidised beds. *Transcr Inst Chem Eng*. 1977;55(October 1977):274-280. http://ci.nii.ac.jp/naid/80014839677/.
34. Rüdisüli M, Schildhauer TJ, Biollaz SMA, Van Ommen JR. Radial bubble distribution in a fluidized bed with vertical tubes. *Ind Eng Chem Res*. 2012;51(42):13815-13824. doi:10.1021/ie3004418

35. Rüdisüli M, Schildhauer TJ, Biollaz SMA, Wokaun A, Ruud van Ommen J. Comparison of bubble growth obtained from pressure fluctuation measurements to optical probing and literature correlations. *Chem Eng Sci*. 2012;74:266-275. doi:10.1016/j.ces.2012.01.045

36. Kobayashi N, Yamazaki R, Mori S. A study on the behavior of bubbles and solids in bubbling fluidized beds. *Powder Technol*. 2000;113(3):327-344. doi:10.1016/S0032-5910(00)00315-6

37. Wang H, Lu Y, Xi K. Bubble behavior in gas–solid bubbling fluidized beds based on EMMS model: Comparison of 2D, Q2D, and 3D simulations. *Chem Eng Res Des*. 2019;149:65-80. doi:10.1016/j.cherd.2019.06.009